Journal of Industrial and Engineering Chemistry 71 (2019) 318–326

Contents lists available at ScienceDirect

Journal of Industrial and Engineering Chemistry

journal homepage: www.elsevier.com/locate/jiec

Laser desorption/ionization mass spectrometry-based compositional analysis of Au–Ag nanoplates synthesized by galvanic replacement and their application for small molecule analysis

Young-Kwan Kim[a,*], Kyunglee Kang[b], Hyungjun Kim[c], Kyungtae Kang[d], Hongje Jang[b,*]

[a] Carbon Composite Materials Research Center, Institute of Advanced Composite Materials, Korea Institute of Science and Technology, 92 Chudong-ro, Bondong-eup, Wanju-gun, Jeollabuk-do 55324, Republic of Korea
[b] Department of Chemistry, Kwangwoon University, 20 Gwangwoon-ro, Nowon-gu, Seoul 01897, Republic of Korea
[c] Department of Chemistry, Incheon National University, 119 Academy-ro, Yeonsu-gu, Incheon 22012, Republic of Korea
[d] Department of Applied Chemistry, Kyung Hee University, Yongin, Gyeonggi-do 446-701, Republic of Korea

ARTICLE INFO

Article history:
Received 17 September 2018
Received in revised form 31 October 2018
Accepted 13 November 2018
Available online 10 December 2018

Keywords:
alloy
nanoparticle
galvanic replacement
laser desorption/ionization
mass spectrometry

ABSTRACT

This paper demonstrates that laser desorption/ionization time-of-flight mass spectrometry (LDI-TOF-MS) can be utilized to analyze the relative atomic composition and photothermal conversion properties of Au–Ag alloy nanoplates synthesized by galvanic replacement reactions. Using Au–Ag alloy nanoplates with various shapes, it is found that the porous structures of the nanoplates affect their photothermal conversion efficiency more than their laser energy absorption capacity does. Based on these findings, the optimized Au–Ag alloy nanoplates can be applied to LDI-TOF-MS of small molecules.
© 2018 The Korean Society of Industrial and Engineering Chemistry. Published by Elsevier B.V. All rights reserved.

Introduction

Matrix-assisted laser desorption/ionization time-of-flight mass spectrometry (MALDI-TOF-MS) is considered one of the most powerful analytical methods for high-molecular weight compounds, such as proteins and synthetic polymers, because of its high-throughput analysis compatibility, high resolution, and sensitivity [1]. For this analytical technique, diverse matrices have been successfully developed, including organic molecules, ionic liquids, and hybrids of organic matrices and nanomaterials [2]. In cases of small molecules such as metabolites and environmental pollutants, matrix-free laser desorption/ionization time-of-flight mass spectrometry (LDI-TOF-MS) has been developed and utilized [3]. The key to matrix-free LDI-TOF-MS is the mediator, which converts laser energy into thermal energy for the desorption/ionization of analytes [3]. As a mediator, various nanomaterials, such as carbon nanomaterials [4], quantum dots [5], and magnetic [6,7], metal [8], and semiconductor nanoparticles, have been extensively incorporated [10]. These nanostructures show great potential as an efficient mediator for LDI-TOF-MS analysis of small molecules thanks to their photothermal conversion and/or photo-induced energy transfer characteristics [10]. In particular, gold [11] and semiconductor nanoparticles [12,13] are considered promising platforms based on their tunable size and surface, which provide a large surface area and affinity for various analytes for preconcentration before LDI-TOF-MS analysis [14].

The areas of application of this technique have expanded to the analyses of chemical structures [15] and photochemical properties of carbon nanomaterials [16] based on its advantages as an analytical tool, such as fast and straightforward analysis, small sample requirements, and no need for pre-treatment. For example, LDI-TOF-MS has been recently applied for the characterization of the photochemical stability and photothermal conversion properties of graphene derivatives [17] and to the chemical structural transition of pitch derivatives on a substrate [18]. These results rely on the characteristic fragmentation behavior of carbon materials upon intense laser irradiation, depending on their chemical structures and photothermal conversion properties.

Because this principle is applicable to most materials with optical absorption near the excitation range of the laser source used in the mass spectrometer, we hypothesized that

* Corresponding authors.
E-mail addresses: youngkwan@kist.re.kr (Y.-K. Kim), hjang@kw.ac.kr (H. Jang).

https://doi.org/10.1016/j.jiec.2018.11.042
1226-086X/© 2018 The Korean Society of Industrial and Engineering Chemistry. Published by Elsevier B.V. All rights reserved.

LDI-TOF-MS analysis can be an effective and useful tool for the characterization of the elemental composition of alloy nanomaterials with small amounts of analytes that exhibit photothermal conversion properties in a simple, rapid, and highly sensitive manner [19]. In this respect, the galvanic replacement reaction, a redox reaction-based post-synthetic nanostructure transformation, should be an appropriate synthetic strategy because of the ability to control the morphology and composition of metal alloy nanostructures [20]. Since an early report that showed the formation of spherical nanoshells with internal voids, it has been widely applied in the manufacturing of distinctive nanostructures, such as nanoworms [21] and porous nanoparticles [22]. The nanoparticles formed by galvanic replacement have an alloy composition between the sacrificial template, e.g., silver (Ag), copper (Cu), or cobalt (Co), and the replacing metal cation, e.g., gold (Au), platinum (Pt), or palladium (Pd) [23]. Considering the recent reports of plasmonic nanoshell-based LDI-TOF-MS analysis [24–26], the distinctive shapes of alloy nanoparticles synthesized by galvanic replacement are quite promising for developing an efficient platform for LDI-TOF-MS analysis of small molecules.

Herein, we attempted LDI-TOF-MS-based elemental composition analysis of Au–Ag nanoplates and confirmed their applicability as a matrix for the analysis of various small molecules. The Au–Ag nanoplates were synthesized with varying elemental compositions and morphologies through reducing agent-assisted galvanic replacement reactions (Fig. 1(a)) and characterized using conventional analytical tools including UV–vis spectroscopy, transmission electron microscopy (TEM), and inductively-coupled plasma mass spectrometry (ICP-MS). The measured properties were comparatively correlated with their LDI-TOF-MS elemental analysis results, and the results implied the potential of LDI-TOF-MS as a tool for characterization of the elemental composition and photothermal conversion properties (Fig. 1(b)). Finally, Au–Ag nanoplates were utilized as a mediator for the LDI-TOF-MS analysis of small compounds to exhibit the correlation between their photothermal conversion properties and LDI efficiency. The results showed that LDI-TOF-MS analysis can be efficiently applied for analysis of the elemental composition and photothermal conversion properties of alloyed nanomaterials, and an optimized Au–Ag nanoplate can be an efficient matrix for LDI-TOF-MS analysis of small molecules.

Experimental section

Materials

Hydrogen tetrachloroaurate(III) hydrate was purchased from Kojima Chemicals Co. (Sayama, Saitama, Japan). Silver nitrate, benzyl bromide, pyridine, trisodium citrate dihydrate, hydrogen peroxide (30%), L-ascorbic acid, and sodium tetrahydroborate were purchased from Junsei (Tokyo, Japan). Arginine, histidine, phenylalanine, glucose, sorbitol, sucrose, norfloxacin, sulfamerazine and cetyltrimethylammonium bromide (CTAB) were purchased from Alfa Aesar (Ward Hill, MA). All chemicals were used as received.

Sacrificial Ag nanoplate synthesis

To the clear 50 mL glass vial, 10 mL of 15 mg mL^{-1} PVP (Mw = 29 kDa) solution, 0.25 mL of 10 mM $AgNO_3$, 16.5 mL of deionized (DI) water, 0.3 mL of 30 mM trisodium citrate dihydrate aqueous solution, and 0.06 mL of 30% hydrogen peroxide was added sequentially under the magnetic stirring (300 rpm) in 30 °C water bath. The Ag nanoseed formation was triggered by addition of 0.25 mL of 100 mM sodium tetrahydroborate solution. The color of mixture immediately changed from transparent into pale-yellow, then finally changed into pale-blue. After sufficient incubation for 3 h, seed-growth is performed without any further purification process. To as-prepared Ag nanoseed, 0.333 mL of 75 mM trisodium citrate dihydrate solution and 1 mL of 100 mM L-ascorbic acid solution was added under vigorous stirring. To the Ag nanoseed solution, growth solution composed of 13 mL of 1 mM $AgNO_3$, 0.081 mL of 100 mM citric acid, and 0.01 mL of 75 mM trisodium citrate dihydrate was added by 0.1 mL sec^{-1} of injection time. By seed-mediated growth of Ag nanoplates from Ag nanoseed, solution color changed into deep-blue. After 10 min of incubation to ensure the growth, Ag nanoplate solution was used as sacrificial template for Au–Ag nanoplates without any further purification process.

Reducing agent-assisted galvanic replacement for Au–Ag nanoplate formation

Sacrificial Ag nanoplate solution was 5 times diluted by appropriate volume of DI water. To the diluted Ag nanoplate solution, 1, 4, 10, and 20 vv% of 1 mM hydrogen tetrachloroaurate(III) solution were injected under vigorous magnetic stirring, respectively. After

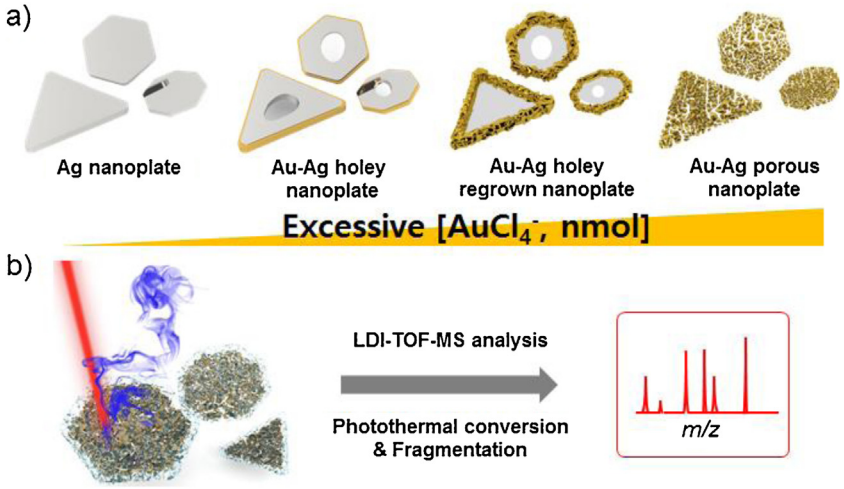

Fig. 1. (a) Schematic diagram of the synthesis of Au–Ag nanoplates by reducing agent-assisted galvanic replacement reaction and (b) subsequent application of them to LDI-TOF-MS analysis.

incubation time (~2 h) at ambient condition, the Au–Ag nanoplates were purified by centrifugation at 9000 rpm for 10 min and washed with DI water for 3 times. Finally, purified Au–Ag nanoplates were concentrated to volume of used Ag nanoplate before dilution.

Galvanic reaction of Ag nanoplates with Au(III) in the presence of CTAB

1 mM hydrogen tetrachloroaurate (III) solution in 0.1 M CTAB was prepared and injected to the sacrificial Ag nanoplate by 7, 10, and 20 vv%. After incubation time (~2 h) at ambient condition, the Au–Ag nanoplates were purified by centrifugation at 9000 rpm for 10 min and washed with DI water for 3 times. Finally, purified Au–Ag nanoplates were concentrated to volume of used Ag nanoplate before dilution.

Synthesis of benzylpyridinium salt (BP)

45.5 mmol of benzyl bromide was added to 37.9 mmol of pyridine with stirring and their reaction mixture was stirred at 50 °C for 12 h. After reaction, the precipitate was formed and it was washed with diethyl ether, filtered, and washed with a large amount of diethyl ether to get BP (95% yield).

LDI-TOF-MS analysis

For compositional analysis of Ag and Au–Ag nanoplates, 1 μL of Ag and Au–Ag nanoplate suspensions were spotted on the surface of a target plate, dried under ambient condition and subjected to LDI-TOF-MS analysis. To obtain total ion intensity and survival yield of BP, 1 μL of 1 mM methanolic solution of BP was spotted on the target plate, mixed with 1 μL of Ag and Au–Ag nanoplate suspensions, dried under ambient condition and subjected to LDI-TOF-MS analysis. For small molecule analysis, 1 μL of 1, 0.1 and 0.01 mM aqueous solutions of arginine, histidine, phenylalanine, glucose, sorbitol, sucrose, norfloxacin and sulfamerazine were spotted on the target plate, mixed with 1 μL of Au–Ag nanoplate (20 vv%), dried under ambient condition and subjected to LDI-TOF-MS analysis.

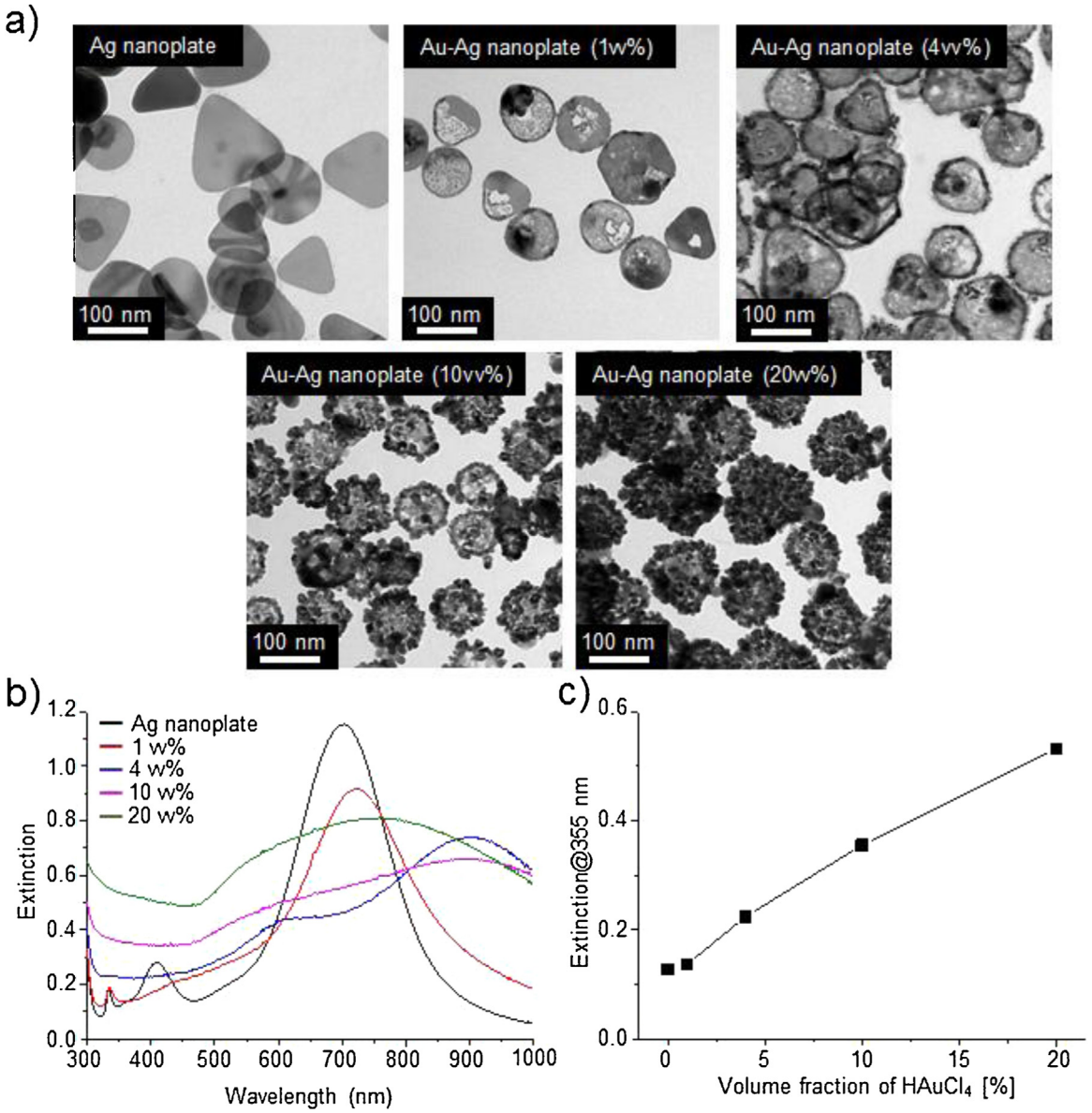

Fig. 2. (a) TEM images, (b) UV–vis spectra and (c) extinction at 355 nm of Ag and Au–Ag nanoplates synthesized by galvanic replacement reaction with different volumes of $AuCl_4^-$ solution. The scale bar is 100 nm.

Characterization

Energy-filtering transmission electron microscope LIBRA 120 (Carl Zeiss, Germany), was used to obtain images of synthesized Au–Ag nanoplates. UV–vis spectrophotometer Lambda 465 (PerkinElmer, USA) was used to obtain UV–vis–NIR extinction spectrum. Inductively coupled plasma mass spectroscopy (ICP-MS) analysis was performed by iCAP-Q (Thermo Electron Corp., USA). Laser desorption/ionization time-of-flight mass spectrometry (LDI-TOF-MS) analysis was conducted with a Bruker Autoflex III (Bruker Daltonics, Germany) equipped with a Smartbeam laser (Nd:YAG, 355 nm, 100 Hz, 100 μJ, 50 μm in its spot diameter at target plate) in positive reflective mode (40% laser power). The accelerating voltage was set at 19 kV and all spectra were obtained by averaging 500 shots.

Results and discussion

A variety of Ag–Au nanoplate derivatives were synthesized using a previously reported reducing agent-assisted galvanic replacement method [27]. Briefly, 1 mM of replacing $AuCl_4^-$ solution, corresponding to either 1, 4, 10, or 20 vv% of the reaction volume, was added to as-synthesized sacrificial Ag nanoplate templates, and the reaction was maintained for 2 h at ambient conditions to enable galvanic replacement and the re-growth process. Considering the stoichiometric redox balance between Au (III) and Ag(I), 1, 4, 10, and 20 vv% reaction conditions could be interpreted as Au/Ag ratios id 0.387, 1.548, 3.871, and 7.742, respectively. TEM images clearly showed the formation of distinctive nanostructures, including holey nanoplates (1 vv%), regrown Au–Ag nanoplates (4 vv%), porous Au–Ag nanoplates (10 vv%), and overgrown porous Au–Ag nanoplates (20 vv%), consistent with our previous study (Fig. 2(a)) [27,28]. All of the obtained Au–Ag alloy nanoplates had similar diameters to the Ag nanoplates used as the template, approximately 80 nm, and it was previously reported that the Au–Ag nanoplates were composed of polycrystalline structures (for high-resolution TEM and FFT images of Au–Ag nanoplates (20 vv%), see Fig. S1) [27,28]. Gradual galvanic replacement occurred with an increasing amount of Au(III) replaced, and structural changes during this process were trackable through UV–vis–NIR analysis (Fig. 2(b and c)). When 1 vv% of Au(III) was added, a weak bathochromic shift (~10 nm) was observed from the tip rounding of Ag nanoplates and the formation of small holes. At 4 vv%, the nanoframe structure was formed as a result of the expansion of the internal holes, and a bathochromic shift followed. The addition of greater than 10 vv% resulted in the formation of porous nanoplates and overgrowth because of the reduction of remaining excess Au(III), and the overall extinction spectrum at wavelengths greater than 500 nm was observed, instead of the characteristic localized surface plasmon resonance (LSPR) of Ag nanoplates or nanoframes (Fig. 2(b)). Along with these changes, the extinction of the synthesized Au–Ag nanoplates at 355 nm, which is an excitation laser wavelength used for LDI-TOF-MS equipment, gradually increased as the galvanic replacement proceeded (Fig. 2(c)).

The synthesized Au–Ag nanoplates were then analyzed via LDI-TOF-MS. The LDI-TOF-MS spectra of the Ag nanoplates showed Ag ion cluster peaks of Ag^+, Ag_2^+ and Ag_3^+ at *m/z* 107, 214 and 321, respectively (Fig. 3(a)) [9]. The relative intensity of each cluster increased in the order of Ag_2^+, Ag^+ and Ag_3^+, a result that has been frequently observed in LDI-TOF-MS analyses of Ag nanoparticles [9]. After galvanic replacement reaction with 1 vv%, new ion peaks of Au^+, $AgAu^+$, Au_2^+ and Ag_2Au^+ at *m/z* 196, 302, 392 and 411, respectively, appeared, with considerable decreases in the relative intensities of Ag_2^+ and Ag_3^+ ion clusters (Fig. 3(a)). This result can be attributed to the increase in Au elemental content on the surface of Ag nanoplates by galvanic replacement, which impedes the formation of large Au ion clusters. At 4 vv%, the relative intensity of

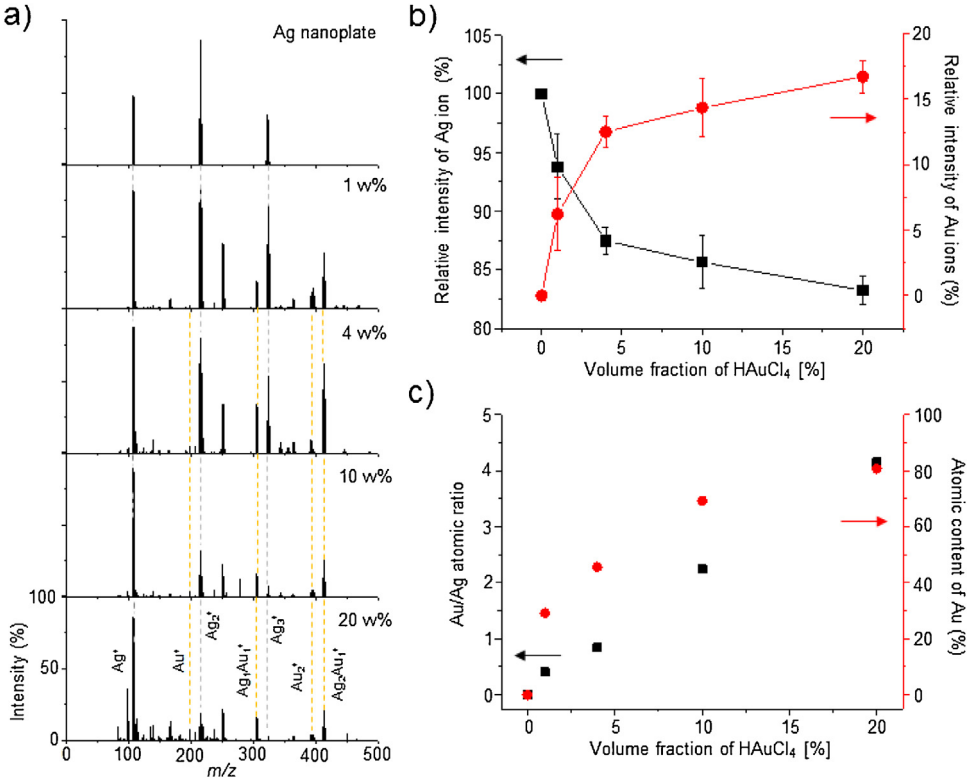

Fig. 3. (a) LDI-TOF-MS spectra of Ag and Au–Ag nanoplates obtained under positive reflection mode. (b) Relative intensities of Ag and Au ions from the LDI-TOF-MS spectra of Ag and Au–Ag nanoplates. (c) Au/Ag atomic ratio and elemental Au content of Ag and Au–Ag nanoplates obtained with ICP-MS analysis.

Ag_2^+ and Ag_3^+ ion clusters with respect to Ag^+ ion clusters further decreased, and the relative intensity of Au ion clusters increased (Fig. 3(a)). This change reflects the progress of the galvanic replacement reaction because the relative atomic Au/Ag ratio in Au–Ag nanoplates obviously increased with the progression of the galvanic replacement reaction. Therefore, the relative intensities of Ag_2^+ and Ag_3^+ ion clusters significantly diminished with increasing relative intensities of Au^+, $AgAu^+$, Au_2^+, and Ag_2Au^+ ion clusters from Au–Ag nanoplates synthesized at the 10 vv% reaction condition (Fig. 3(a)). Finally, at 20 vv%, the relative intensities of Au^+, $AgAu^+$, Au_2^+, and Ag_2Au^+ ion clusters became comparable to Ag_2^+ and Ag_3^+ ion clusters (Fig. 3(a)). These intensity changes in detected metal ion clusters clearly suggested that LDI-TOF-MS analysis can be directly used to quantify the relative atomic ratio of alloy nanomaterials. Then, the total relative intensities of Ag and Au ion clusters from Ag and Au–Ag nanoplates were examined by summing all intensities of Ag ion clusters (Ag^+, Ag_2^+, Ag_3^+, Ag_2Au^+, and $AgAu^+$) and Au ion clusters (Au^+, Ag_2Au^+, and $AgAu^+$), respectively. The relative intensity of Ag versus Au ion clusters was 100% for Ag nanoplates without galvanic replacement (Fig. 3(b)). As galvanic replacement proceeded from 1 to 20 vv%, the relative intensity of Ag ion clusters gradually decreased, from $93.8 \pm 2.8\%$ to $83.3 \pm 1.3\%$; thus, the relative intensity of Au ion clusters increased from $6.2 \pm 2.8\%$ to $16.7 \pm 1.3\%$ (Fig. 3(b)). These results further support the idea that LDI-TOF-MS can be used as an analytical tool to determine the relative quantitative elemental composition of alloy nanomaterials. The few unassigned mass peaks in the LDI-TOF-MS spectra of Au–Ag nanoplates might originate from the fragmentation of surface-adsorbed residual polyvinylpyrrolidone (PVP), and this fragmentation implies that the photothermal conversion efficiency of Au–Ag nanoplates with the 355-nm wavelength laser equipped in the mass spectrometer was enhanced with the galvanic replacement reaction because of the increase in the laser energy absorption capacity and amount of porous structures (Fig. 2(c)).

To determine the exact atomic ratio of Au–Ag nanoplates using a standard analytical tool, ICP-MS analyses of Ag and Au–Ag nanoplates were carried out for comparison with LDI-TOF-MS analysis results. The Au element was not detected from the Ag nanoplate, but, after the 1 vv% galvanic replacement reaction, the elemental composition of Au increased to 29.2% (Fig. 3(c)). As the galvanic replacement reaction proceeded to 20 vv%, the elemental composition of Au increased considerably, to 80.6% (Fig. 3(c)); this value is much higher than the relative intensity of Au ion clusters in the LDI-TOF-MS spectrum (Fig. 3(b)). This deviation might stem from the difference between Ag and Au elements in terms of ionization energy, laser energy absorption capacity, and heat capacity, which critically affect the intensity of metal ion clusters in LDI-TOF-MS spectra [29]. However, it is noteworthy that the increasing tendency of the relative Au ion cluster intensities in the LDI-TOF-MS spectra of Ag and Au–Ag nanoplates concurred in the ICP-MS analysis results. This result shows the potential of LDI-TOF-MS for the elemental composition analysis of alloy nanomaterials.

The photothermal conversion efficiency of Ag and Au–Ag nanoplates was explored using benzylpyridinium salt (BP) as a thermometer molecule. The applicability of nanomaterials as a mediator for LDI-TOF-MS analysis of small molecules can be estimated on the basis of the laser desorption/ionization (LDI) behavior of BP [16]. The total ion intensity (TII) and survival yield (SY) of BP can be obtained by summing BP and its fragmented ion intensities and dividing the BP ion intensity by the TII value, respectively (Fig. 4(a and b)). TII and SY are directly related to the LDI efficiency and soft-ionization potential of the nanomaterials [4]. When a methanolic solution of BP was mixed with aqueous suspensions of Ag and Au–Ag nanoplates on the target plate, a spot of the mixture was homogeneously formed without formation of a "coffee ring" (Fig. S2); thus, uniform mass signals of BP could be obtained (Fig. 4(a and b)). With Ag nanoplates, there was no mass signal of BP, but there were weak signals from Ag ion clusters, indicating that Ag nanoplates do not assist the LDI of BP (Fig. 4(a)).

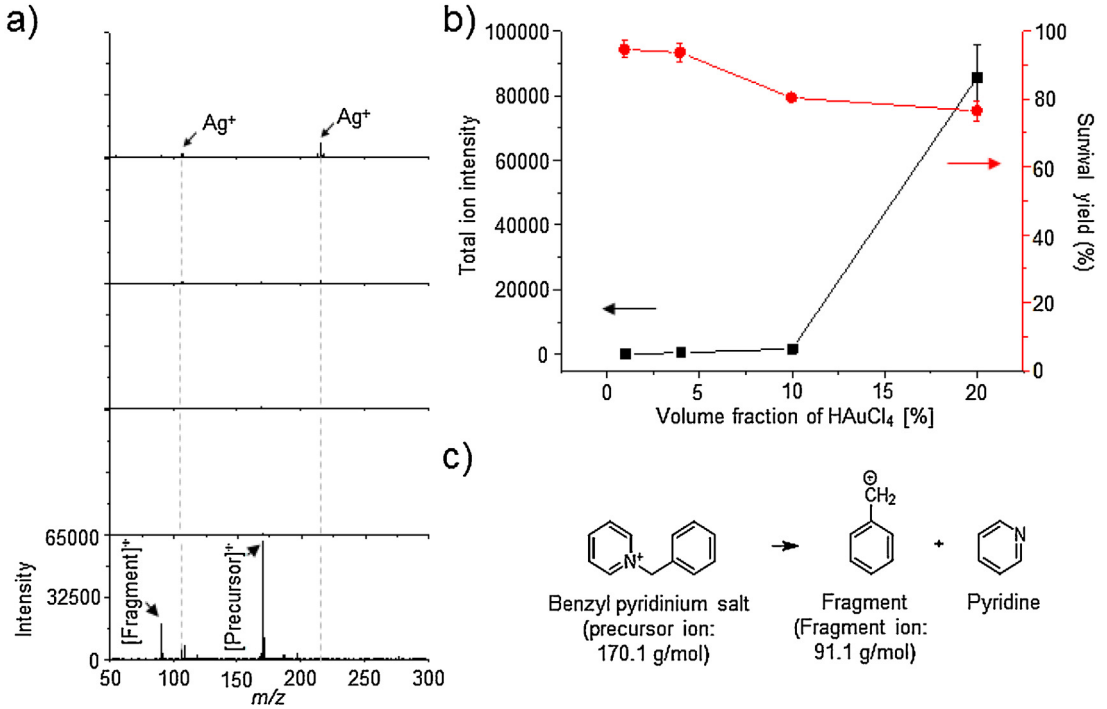

Fig. 4. (a) LDI-TOF-MS spectra, (b) TII and SY values of BP obtained with Ag and Au–Ag nanoplates, and (c) fragmentation process of BP during LDI-TOF-MS analysis under positive reflection mode.

Conversely, mass signals of BP were detected with Au–Ag nanoplates (1 vv%), and the TII value was 104 ± 10 (Fig. 4(a)). This drastic change is noteworthy, considering that the laser energy absorption capacity of the Ag nanoplate is comparable with that of the Au–Ag nanoplate (1 vv%) (Fig. 2(b and c)). With progression of the galvanic replacement up to 20 vv%, the TII value of Au–Ag nanoplates increased dramatically and finally reached 85586 ± 9970 (Fig. 4(a and c)). This result is coherent with the LDI-TOF-MS spectrum of Au–Ag nanoplates (20 vv%), as this enhanced LDI efficiency of Au–Ag nanoplates with the galvanic replacement reaction can result in undesirable fragmentation of surface-adsorbed residual polymers (Fig. 3(a)). Whereas the TII value increased with the progression of the galvanic replacement reaction, the SY value of Au–Ag nanoplates gradually decreased, from 94.6 ± 2.5% (at 1 vv%) to 76.7 ± 3.0% (at 20 vv%) (Fig. 4(c)). This inverse tendency for TII and SY proves that the LDI of BP on Au–Ag nanoplates proceeded with the photothermal process, and the photothermal conversion efficiency of Au–Ag nanoplates was enhanced as the galvanic replacement reaction progressed.

Another set of Au–Ag alloy nanoplates, with different morphologies but similar elemental composition, was synthesized using a modified galvanic replacement reaction. In the conventional galvanic replacement reactions, three Ag atoms were required to reduce one Au(III) ion, forming porous Au–Ag nanoplates, but it is known that Au(I) ions form a dense hollow nanoshell containing only a few pores for ion discharge as a result of the one-to-one redox reaction balance between the participants. Au(I) ions were used as a replacing agent to synthesize Au–Ag nanoplates with less porous structure than Au–Ag nanoplates synthesized by the reducing agent-assisted galvanic replacement reaction. To accomplish this, 1 mM $AuCl_4^-$ in 0.1 M CTAB solution was added as Au(I) ions to the suspension of sacrificial Ag nanoplates at concentrations of 7 and 20 vv%, interpreted as respective stoichiometric Au/Ag ratios of 0.90 and 2.58. TEM images of the synthesized Au–Ag nanoplate with surface-adsorbed CTAB (CTAB_Au–Ag nanoplates) showed that nano-sized pores were formed on the basal plane of the Ag nanoplates at 7 vv%, while protruded spikes were grown on the Ag nanoplates at 20 vv% (Fig. 5(a)). In their UV–vis–NIR spectra, shell thickening and protruding gradually led to a hypsochromic shift of the LSPR peak from 994 nm (7%) to 785 nm (20%), which is likely due to the gradual weakening of hybridization caused by an increase in the exterior–interior surface distance (Fig. 5(b)). Their laser energy absorption capacity at 355 nm also gradually increased as the galvanic replacement reaction progressed (Fig. 5(c)). The diversity of morphology and laser energy absorption capacity of CTAB_Au–Ag nanoplates (7 and 20 vv%) can facilitate exploration of the correlation between the effects of morphology and laser energy absorption capacity on the LDI-TOF-MS behavior of Au–Ag alloy nanoplates.

The synthesized CTAB_Au–Ag nanoplates were then analyzed using LDI-TOF-MS. The LDI-TOF-MS spectrum of Ag nanoplates exhibited features quite similar to those in Fig. 3(a) (Fig. 6(a)). After the galvanic replacement reaction with Au(I) (7 vv%), the Au ion cluster peaks (Au^+, $AgAu^+$, Au_2^+, and Ag_2Au^+) were clearly detected, with a new strong peak at *m/z* 284 corresponding to surface-adsorbed CTAB and a sharp decrease in the relative intensities of Ag_2^+ and Ag_3^+ ion clusters (Fig. 6(a and b)). As the galvanic replacement reaction proceeded to 20 vv% of Au(I), the relative intensity of Au ion clusters increased with a decrease in the relative intensity of the Ag ion clusters (Fig. 6(a and b)). This tendency is well matched with the LDI-TOF-MS analysis of Au–Ag nanoplates

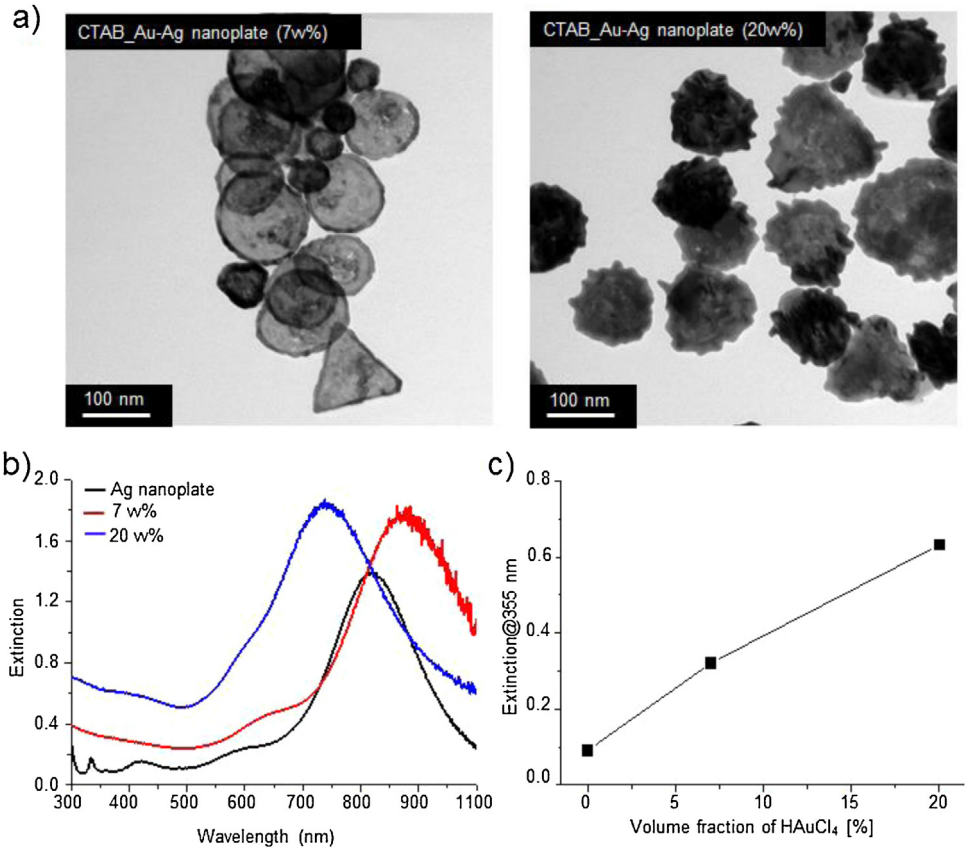

Fig. 5. (a) TEM images, (b) UV–vis spectra and (c) extinction at 355 nm of Ag and Au–Ag nanoplates synthesized by galvanic replacement reaction with different volumes of $AuBr_2^-$ solution.

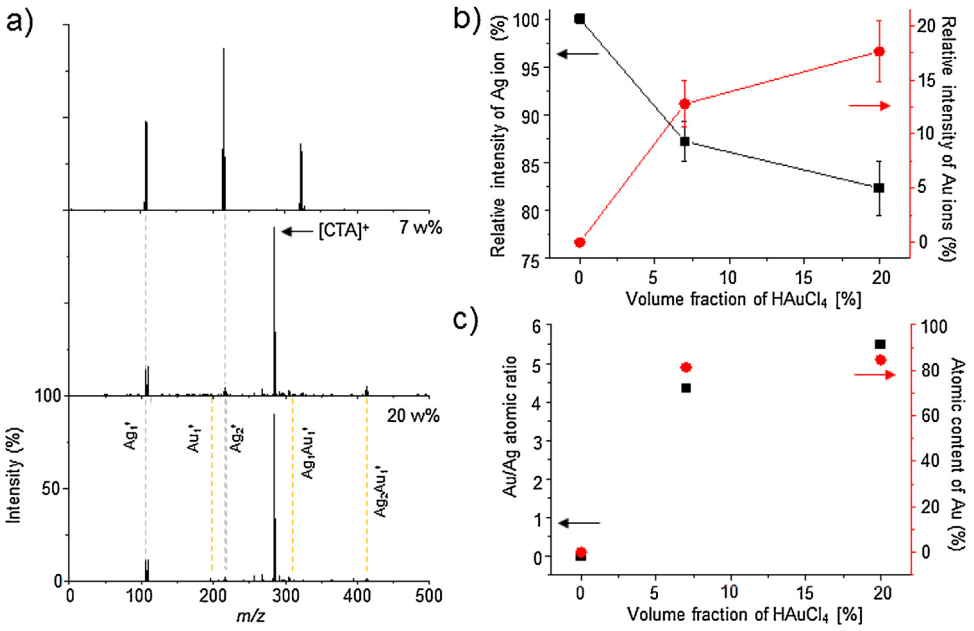

Fig. 6. (a) LDI-TOF-MS spectra of Ag and CTAB_Au–Ag nanoplates obtained under positive reflection mode. (b) Relative intensities of Ag and Au ion clusters from the LDI-TOF-MS spectra of Ag and CTAB_Au–Ag nanoplates. (c) Au/Ag atomic ratio and elemental Au content of Ag and CTAB_Au–Ag nanoplates obtained with ICP-MS analysis.

synthesized by the reducing agent-assisted galvanic replacement reaction and also indicates that the relative atomic ratio of Ag and Au in Au–Ag alloy nanoplates is reflected in their LDI-TOF-MS spectra, regardless of their morphology. ICP-MS analysis of Ag and CTAB_Au–Ag nanoplates was also carried out to validate the LDI-TOF-MS analysis results. While the Au element was not detected within the Ag nanoplates, the elemental composition of Au in CTAB_Au–Ag nanoplates (7 vv%) increased to 81.3%, and it further increased to 84.6% for the 20 vv% galvanic replacement reaction (Fig. 6(c)). This value is also much higher than the relative intensity of Au ion clusters in the LDI-TOF-MS spectra of CTAB_Au–Ag nanoplates (Fig. 6(b)), but is in agreement with the characterization results of Ag and Au–Ag nanoplates synthesized by the reducing agent-assisted galvanic replacement reaction. Therefore, this result further confirms the potential applicability of LDI-TOF-MS for the elemental composition analysis of alloy nanomaterials.

To investigate the effects of morphology and laser energy absorption capacity of the Au–Ag alloy nanoplates on their photothermal conversion efficiency, LDI-TOF-MS analysis of BP was carried out in the presence of CTAB_Au–Ag nanoplates. Unexpectedly, CTAB_Au–Ag nanoplates (7 vv%) induced highly efficient LDI of BP (Fig. 7(a)). The TII value was 95270 ± 9400, which is even higher than that for Au–Ag nanoplates (20 vv%) synthesized by the reducing agent-assisted galvanic replacement reaction (85586 ± 9970) (Fig. 7(b)). Interestingly, the TII value of CTAB_Au–Ag nanoplates decreased to 83206 ± 11013 as the galvanic replacement reaction proceeded to 20 vv% of Au(I) (Fig. 7(b)), although the laser energy absorption capacity of the CTAB_Au–Ag nanoplate (7 vv%) (extinction at 355 nm: 0.32) was two times lower than that of the CTAB_Au–Ag nanoplate (20 vv%) (extinction at 355 nm: 0.63). Conversely, the SY value of the CTAB_Au–Ag nanoplate (7 vv%) was 67.6 ± 1.4%, and this value increased to 71.5 ± 3.6% at 20 vv% (Fig. 7(b)). This tendency is completely opposite that of the Au–Ag nanoplates synthesized by the reducing agent-assisted galvanic replacement reaction, because, in their case, the TII value was enhanced, whereas the SY value decreased with their extinction at 355 nm as a result of excess galvanic replacement. This result implies that the high TII was not simply derived from the extinction and degree of galvanic replacement of Au–Ag alloy nanoplates. Based on the morphology, laser energy absorption capacity, and elemental composition of CTAB_Au–Ag nanoplates, we conclude that the morphological effect from the small internal pores on CTAB_Au–Ag nanoplates (7 vv%) played a more critical role in the LDI process compared with the laser energy absorption capacity at 355 nm and the elemental composition. This indicates the importance of structural porosity for the photothermal conversion efficiency of Au–Ag nanoplates.

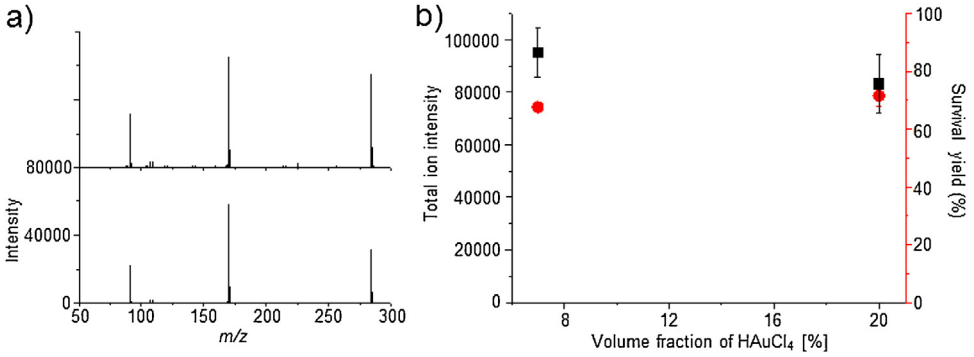

Fig. 7. (a) LDI-TOF-MS spectra and (b) TII and SY values of BP obtained with Ag and CTAB_Au–Ag nanoplates under positive reflection mode.

To confirm the practical applicability of Au–Ag nanoplates as a mediator for LDI-TOF-MS analysis of small molecules, the Au–Ag nanoplates (20 vv%) were utilized instead of CTAB_Au–Ag nanoplates (7 vv%) because the strong peak from CTAB interfered with LDI-TOF-MS analysis of small molecules (Fig. S3). Amino acids, saccharides, and antibiotics were selected as model analytes because they are closely related to metabolic diseases and thus important targets of LDI-TOF-MS analysis. To accomplish this, 1 nmol each of arginine, histidine, phenylalanine, glucose, sorbitol, sucrose, norfloxacin, and sulfamerazine in water was mixed with Au–Ag nanoplates on a target plate and subjected to LDI-TOF-MS analyses. All small molecules were successfully detected with Au–Ag nanoplates as cationic adducts with proton, sodium, and/or potassium, such as *m/z* 175 $[Arg+H]^+$, 197 $[Arg+Na]^+$, 178 $[His+Na]^+$, 200 $[His+2Na]^+$, 166 $[Phe+H]^+$, 188 $[Phe+Na]^+$, 204 $[Phe+K]^+$, 211 $[Phe+2Na]^+$, 203 $[glucose+Na]^+$, 205 $[sorbitol+Na]^+$, 365 $[sucrose+Na]^+$, 342 $[norfloxacin+Na]^+$, 358 $[norfloxacin+K]^+$, 287 $[sulfamerazine+Na]^+$, 303 $[sulfamerazine+K]^+$, and 309 $[sulfamerazine+2Na]^+$ (Fig. 8). The accuracy, resolution, signal to noise ratio (S/N), average signal intensity, and relative standard deviation (RSD) from the LDI-TOF-MS spectra of small molecules are summarized in Table 1. Most of the small molecules were not detected using the Au–Ag nanoplates synthesized at other reaction conditions. The detectable concentration of small molecules was 10 pmol with Au–Ag nanoplates (20 vv%) (Fig. S4), which is comparable to that using carbon nanomaterials-based LDI-TOF-MS platforms [30]; this result suggests that Au–Ag nanoplates can be used for the LDI-TOF-MS analyses of small molecules.

Table 1
The accuracy, resolution, S/N, average intensity and RSD values calculated from the LDI-TOF-MS spectra of small molecules obtained with Au–Ag nanoplate (20 vv%) under positive reflection mode.

	Accuracy (ppm)	Resolution	S/N	Average intensity	RSD(%)
Arginine	57	3645	167	4103	21.8
Histidine	50	4287	513	10314	19.5
Phenylalanine	15	4217	343	7188	19.6
Glucose	93	4617	566	20749	10.3
Sorbital	121	3935	612	14731	15.5
Sucrose	471	7722	188	2824	10.2
Norfloxacin	417	6019	603	16804	25.1
Sulfamerazine	348	5475	937	13032	25.3

Conclusion

In conclusion, Au–Ag nanoplates with varying atomic ratios of Au and Ag were synthesized by galvanic replacement reactions under various different conditions and characterized with conventional analytical tools such as UV–vis, TEM, and ICP-MS. Then, the Au–Ag nanoplates were thoroughly analyzed with LDI-TOF-MS techniques to explore their fragmentation behavior, photothermal conversion efficiency, and applicability as a mediator for LDI-TOF-MS analysis of small molecules. LDI-TOF-MS analysis results were systematically compared with those obtained with conventional analytical tools. Taken together, the results suggest that LDI-TOF-MS analysis can be utilized to estimate the relative elemental composition and photothermal conversion

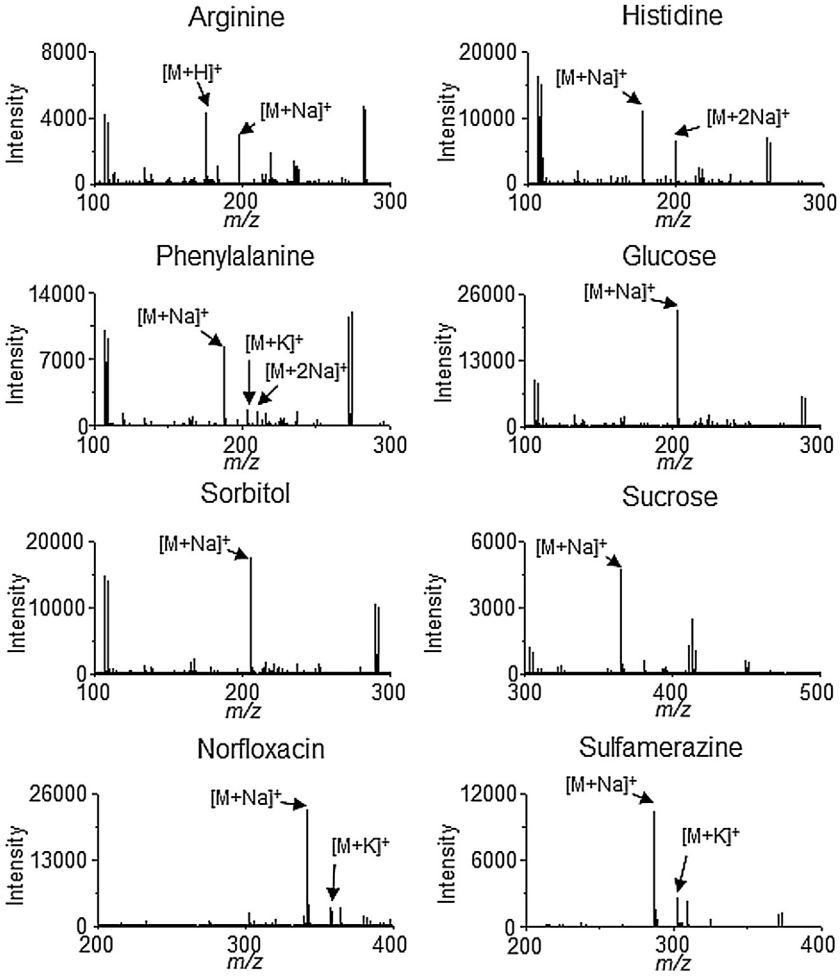

Fig. 8. (a) LDI-TOF-MS spectra of small molecules obtained with Au–Ag nanoplate (20 vv%) under positive reflection mode.

properties of alloy nanomaterials, and these materials can be applied for LDI-TOF-MS analysis of small molecules. Based on our findings, we believe that this study provides an important and fundamental insight and adds another practical tool to investigate the chemical structures and photochemical properties of metallic nanomaterials.

Acknowledgments

This work was supported by a grant from the Korea Institute of Science and Technology Institutional program, the Carbon Cluster Development Program (10083586), the KIAT (Korea Institute for Advancement of Technology) grant (N0000992) funded by the Ministry of Trade, Industry and Energy, Republic of Korea, and the National Research Foundation of Korea (NRF) funded by the Ministry of Science, ICT and Future Planning (2016M3A7B4900119, 2016M3A7B4905619) and Korean government (Grant No. NRF-2016R1C1B1008090).

Declarations of interest

None.

Appendix A. Supplementary data

Supplementary data associated with this article can be found, in the online version, at https://doi.org/10.1016/j.jiec.2018.11.042.

References

[1] M. Karas, F. Hillenkamp, Anal. Chem. 60 (1988) 2299.
[2] H.N. Abdelhamid, Trends Anal. Chem. 89 (2017) 68.
[3] D.S. Peterson, Mass Spectrom. Rev. 26 (2007) 19.
[4] Y.-K. Kim, D.-H. Min, ACS Appl. Mater. Interfaces 4 (2012) 2088.
[5] H.N. Abdelhamid, Z.Y. Chen, H.F. Wu, Anal. Bioanal. Chem. 409 (2017) 4943.
[6] H.N. Abdelhamid, Y.C. Lin, H.F. Wu, RSC Adv. 7 (2017) 41585.
[7] H.N. Abdelhamid, Y.C. Lin, H.F. Wu, Microchim. Acta 184 (2017) 184.
[8] J.A. McLean, K.A. Stumpo, D.H. Russell, J. Am. Chem. Soc. 127 (2005) 5304.
[9] J. Sekuła, J. Nizioł, W. Rode, T. Ruman, Analyst 140 (2015) 6195.
[10] H.N. Abdelhamid, Microchim. Acta 185 (2018) 200.
[11] S.K. Kailasa, H.F. Wu, Analyst 137 (2012) 1629.
[12] S.K. Kailasa, K. Kiran, H.F. Wu, Anal. Chem. 80 (2008) 9681.
[13] S.K. Kailasa, H.F. Wu, Analyst 135 (2010) 1115.
[14] S.K. Kailasa, H.F. Wu, Trends Anal. Chem. 65 (2015) 54.
[15] K. Yoshimura, L. Przybilla, S. Ito, J.D. Brand, M. Wehmeir, H.J. Räder, K. Müllen, Macromol. Chem. Phys. 202 (2001) 215.
[16] H.W. Tang, K.M. Ng, W. Lu, C.M. Che, Anal. Chem. 81 (2009) 4720.
[17] Y.-K. Kim, D.-H. Min, Chem. Eur. J. 21 (2015) 7217.
[18] J.-S. Lee, Y.-K. Kim, J.Y. Hwang, H.-I. Joh, C.R. Park, S. Lee, Carbon 121 (2017) 479.
[19] B. Yan, Y. Jeong, L.A. Mercante, G.Y. Tonga, C. Kim, Z.J. Zhu, R.W. Vachet, V.M. Rotello, Nanoscale 5 (2013) 5063.
[20] Y. Sun, B.T. Mayers, Y. Xia, Nano Lett. 2 (2002) 481.
[21] H. Jang, Y.-K. Kim, D.-H. Min, Chem. Commun. 53 (2017) 1385.
[22] H. Jang, D.-H. Min, ACS Nano 9 (2015) 2696.
[23] X. Xia, Y. Wang, A. Ruditskiy, Y. Xia, Adv. Mater. 25 (2013) 6313.
[24] J. Lee, J. Lee, T.D. Chung, W.S. Yeo, Anal. Chim. Acta 736 (2012) 1.
[25] L. Huang, J. Wan, X. Wei, Y. Liu, J. Huang, X. Sun, R. Zhang, D.D. Gurav, V. Vedarethinam, Y. Li, R. Chen, K. Qian, Nat. Commun. 8 (2017) 220.
[26] X. Sun, L. Huang, R. Zhang, W. Xu, J. Huang, D.D. Gurav, V. Vedarethinam, R. Chen, J. Lou, Q. Wang, J. Wan, K. Qian, ACS Cent. Sci. 4 (2018) 223.
[27] S. Kang, K. Kang, H. Huh, H. Kim, S.-J. Chang, T.J. Park, K.S. Chang, D.-H. Min, H. Jang, ACS Appl. Mater. Interfaces 9 (2017) 35268.
[28] S. Kang, W. Shin, K. Kang, M.-H. Choi, Y.-J. Kim, Y.-K. Kim, D.-H. Min, H. Jang, ACS Appl. Mater. Interfaces 10 (2018) 13819.
[29] C.K. Chiang, W.T. Chen, H.T. Chang, Chem. Soc. Rev. 40 (2011) 1269.
[30] Y.K. Kim, H.K. Na, S.J. Kwack, S.R. Ryoo, Y. Lee, S. Hong, S. Hong, Y. Jeong, D.H. Min, ACS Nano 5 (2011) 4550.